Rovibrational excitation of rare-gas dimers by electron impact

E. P. Seidel[*] and F. Arretche[†]

Departamento de Física, Universidade Federal de Santa Catarina, 88040-900 Florianópolis, Santa Catarina, Brazil

Electron scattering by rare-gas dimers is studied for very low incident energies using the zero range potential (ZRP) method. Beyond the traditional ZRP, we consider an alternative formulation accounting for the atomic polarization, inspired in the modified effective range theory. The scattering calculations are reported in fixed nuclei, rigid rotor, and rovibrational approximations, the first two being analytical. An expression for the electron-molecule scattering length is obtained. We find that short-range interactions are the dominant mechanism for rotational transitions in electron scattering by rare-gas dimers, while the long-range interactions may be neglected. Our results show how the elastic, rotational, and rovibrational cross sections depend on the electron-atom scattering length, on the molecular parameters, and also on the inclusion of polarization effects. The principle of detailed balance is discussed in the context of the ZRP method. Finally, we show that the rovibrational coupling considerably affects the rotational cross sections when the rotational constant becomes comparable to the vibrational constant.

I. INTRODUCTION

When an environment composed by noble gas atoms finds proper thermodynamic conditions, there exists a probability that these atoms interact between themselves through van der Waals forces, forming dimers [1,2]. The rare-gas dimers have been the subject of a broad spectroscopic investigation performed by Tanaka and Yoshino for He_2, Ne_2, and Ar_2 [3–5], by Tanaka *et al.* for Kr_2 [6], and by Freeman *et al.* for Xe_2 [7]. Since then, such dimers have been extensively studied in order to establish potentials that properly describe the molecular properties (see, for example, Slavíček *et al.* [8] and Tang and Toennies [9]). Such a task has shown to be a difficult one. For He_2, for instance, Cybulski and Toczylowski reported an *ab initio* potential that is not even deep enough to support a vibrational bound state [10], while it does exist for the potential calculated by Janzen and Aziz [11].

As far as we could verify, very few explicit studies about electron scattering by neutral van der Waals dimers have been reported in literature so far. Sweeping the 8.0–8.9 energy-loss range and paying attention to the Feshbach resonances associated to the Xe $^3P_2$ and $^3P_1$ atomic lines, Allan measured the electron impact spectra of Xe_2 and Xe_n ($n \sim 3$, 4) [12] and observed that such structures are practically absent in the dimers. More recently, Blanco and Garcia [13] computed electron-Ar_2 scattering cross sections between 1 and 500 eV using the screening corrected additivity rule combined with the independent atom representation. This technique is able to generate elastic, inelastic, and total cross sections but does not take into account the rotational and vibrational dynamics of the target. On the other side, through the years, more attention has been given to the problem of electron scattering by rare-gas ionized dimers, the so-called dissociative recombination: $e^- + R_2^+ \rightarrow R + R + $ kinetic energy [14–18].

Investigations on $e^- + X_2$ ($X =$ He, Ne, Ar, Kr, and Xe) dimers are, in fact, scarce. In principle, the associated cross sections could be calculated with well-established methods like the R matrix [19] or the complex Kohn [20]. The computation of electron-molecule cross sections is specially hard for very low incident electron energies, mainly about what concerns the incorporation of the target-projectile correlation-polarization effects and the proper evaluation of the vibrational and rotational couplings.

Considering the very-low-energy regime, we find a suitable method known as the zero range potential (ZRP) [21]. In this approach the effect of the scattering potential is reduced to a boundary condition. The greatest advantage of using the ZRP is that the calculation is strongly simplified when compared to more sophisticated treatments, and analytical solutions may be found for some particular cases. It works as a semiempirical method because the working expressions for the cross sections depend on parameters like the electron-atom scattering length or the atomic dipole polarizability in such a way that it is possible to investigate how the cross sections vary with different values for each atomic and molecular parameter.

ZRP is a successful methodology that has been applied to the electron-molecule scattering problem. Drukarev and Yurova used it combined with the adiabatic approximation to calculate rotational and vibrational cross sections for electron-H_2, Li_2, Na_2, and K_2 impact [22]. In a similar way, Ostrovsky and Ustimov obtained the exact solution of the particle-rigid-rotor scattering problem [23], based on the ZRP formulation. Later, Gribakin demonstrated, using the ZRP, that positron annihilation with molecules can be enhanced due to Feshbach vibrational resonances [24]. Finally, Leble and Yalunin applied the ZRP to calculate the $X^1\Sigma_g^+ \rightarrow a^3\Sigma_g^+$ electronic and vibrational excitation cross sections of H_2 by electron impact [25,26].

―――――――――
[*]e.p.seidel@posgrad.ufsc.br
[†]f.arretche@ufsc.br

For this work, we consider the traditional ZRP prescription and a modified one in which the effect of the atomic polarizability is explicitly accounted, inspired in the modified effective range theory (MERT) [27], originally conceived to treat electron-atom scattering. The scattering cross sections are calculated in the fixed nuclei, the rigid rotor (RRA) and the rovibrational (RVA) approximations, taking the rotational and vibrational dynamics explicitly. This formulation permits a direct identification of an electron-molecule scattering length, from the equilibrium internuclear distances and the electron-atom scattering lengths.

This paper is organized as follows: Section II presents the theory developed for this work. Section III brings the atomic and molecular parameters used in the calculations. Section IV shows the results and discussion. Finally, we present our conclusions at the end, in Sec. V. Atomic units are used throughout the paper.

II. THEORY

The ZRP approximation becomes physically interesting when the particle de Broglie wavelength is much greater than the potential range. In other words, it is a good approximation for very small incident momentum particles. Considering the potential field of order $\sim 8\ a_0$ (the largest internuclear equilibrium distance corresponding to Xe_2 [9]), we apply such methodology to incident electron energies up to 100 meV.

The application of the ZRP method to van der Waals homonuclear rare-gas dimers is very convenient. This is because each rare-gas atom in the dimer causes only a small perturbation in the second one. As a consequence, it is possible to model the dimer as two "individual" atoms under an internuclear distance constraint $\vec{R} = \vec{R}_1 - \vec{R}_2$, where $\vec{R}_i$ locates the ith nucleus [24,28].

A. ZRP to electron – Atom

Following Gribakin [24], it is important to understand how ZRP works for electron-atom scattering. For small momenta, the electron-atom interaction is described in ZRP approximation by the boundary condition [21]

$$\frac{1}{r\psi(r)}\frac{d[r\psi(r)]}{dr}\bigg|_{r\to 0} = -\kappa_0, \tag{1}$$

where κ_0 is a parameter and the atom, represented by the ZRP, is placed at the origin. In order to determine κ_0, we use the fact that, except at the scattering center, the electron is described as a free particle and its wave function is

$$\psi(r) = N(k)\frac{\sin(kr + \delta_0)}{r}, \tag{2}$$

where k is the electron momentum, $N(k)$ is a normalization factor which depends on k, and δ_0 is the s-wave phase shift. From boundary condition (1), one gets

$$k\cot\delta_0 = -\kappa_0. \tag{3}$$

In the limit $k \to 0$, it is known from effective range theory (ERT) [29,30] that

$$\kappa_0 = -k\cot\delta_0 \simeq \frac{1}{A}, \tag{4}$$

where A is identified as the electron-atom scattering length. One may observe that the original ERT was generalized taking account terms related to the long-range polarization potential $(-\alpha_d/2r^4)$, where α_d is the dipole polarizability of the atom ([31], Sec. 12.2), introducing the modified effective range theory (MERT) [27,32]. The results provided by MERT have shown to be more accurate for electron-atom scattering than the ERT results. It leads us to conjecture that the inclusion of such terms in Eq. (4) may improve the results for both individual atoms and dimer molecules in the ZRP method as well. For these reasons, we propose a ZRP parameter dependent on momentum $\kappa_0(k)$, inspired in the MERT expansion [32]:

$$\kappa_0(k) = -k\cot\delta_0 \simeq \frac{1}{A} - \frac{\pi\alpha_d}{3A^2}k - \frac{4\alpha_d}{3A}k^2\ln(k). \tag{5}$$

We would like to emphasize this is not the first time that a ZRP parameter dependent on k is found in literature. Fedorov and Jensen, for example, have considered the ERT expansion with a similar strategy [33].

In order to make the discussion easier throughout the paper, we shall denominate the prescription that considers the target polarizability through Eq. (5) zero range potential with polarization as ZRPP, while the original one represented by Eq. (4) simply as ZRP. Figure 1 shows the s-wave phase shifts for electrons scattered by Ne and Xe atoms considering the ZRP and ZRPP models. The results are compared to the best MERT fitting reported by Shigemura *et al.* [34] for Ne and Kurokawa *et al.* [35] for Xe able to reproduce their experimental cross sections. As expected for atoms, the ZRPP method improves the s-wave phase shifts when compared to the ZRP ones. The s-wave cross section is calculated using

$$\sigma(k) = \frac{4\pi}{k^2 + \kappa_0^2(k)}$$
$$\approx 4\pi A^2\left(1 + \frac{2\pi\alpha_d}{3A}k + \frac{8\pi\alpha_d\ln k}{3}k^2 + \cdots\right), \tag{6}$$

which works for both ZRP and ZRPP formulations, for small momenta [21,24]. This equation is similar to the ones reported by O'Malley [36] and later by Mitroy [37], which supports the hypothesis that the ZRPP model improves the results for electron-atom cross sections and brings it closer to the MERT ones.

We would like to call attention to a subtlety found in the electron-Ne investigation. There is a vanishing of the ZRPP parameter $\kappa_0(k)$ at $\pi\alpha_d k/3A^2 \approx 1/A$ [see Eq. (5)]. This effect becomes considerable at energies above ~ 15 meV, and, because of that, we focus on energies up to 10 meV for this system. No such problem occurred with the other atoms.

B. Electron – Rare-gas dimers

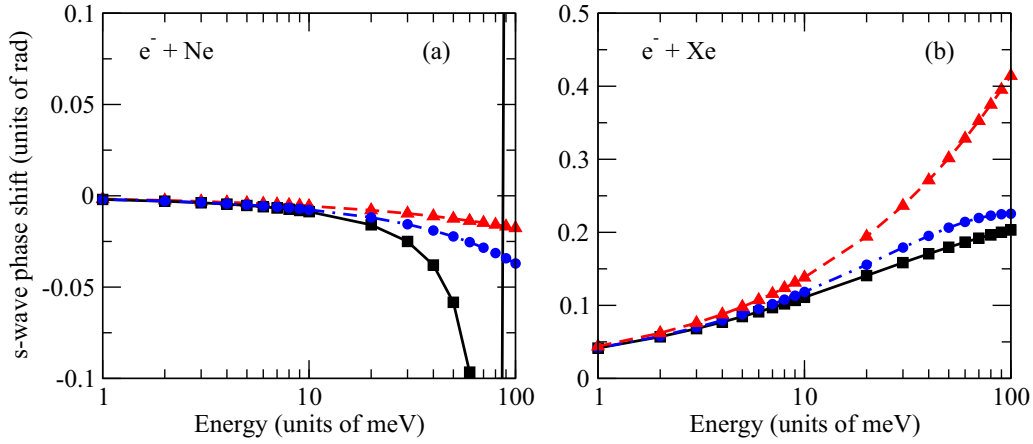In this section, we denote the rare-gas dimer simply as a molecule. According to ZRP, the electron-molecule scattering

FIG. 1. s-Wave phase shifts as a function of incident energy for $e^- + $ Ne with A (electron-atom scattering length)$=0.206$ (panel a) and $e^- +$ Xe with $A = -5.13$ (panel b). The polarizability value used for each atom is presented in Table III. Dashed line with triangles up: calculated with zero range potential (ZRP) [Eq. (4)]; solid line with squares: calculated with zero range potential with polarization (ZRPP) [Eq. (5)]; dashed-dot line with circles: MERT fitting from experimental measurement at small energies [34,35].

wave function outside the atoms [24,28] is written as

$$\psi(\vec{r}) = e^{i\vec{k}_{\nu_i} \cdot \vec{r}} \Psi_{\nu_i}(\vec{R}) + \sum_{\nu'} A_{\nu'} \frac{e^{ik_{\nu'}|\vec{r} - \vec{R}_1|}}{|\vec{r} - \vec{R}_1|} \Psi_{\nu'}(\vec{R})$$

$$+ \sum_{\nu'} B_{\nu'} \frac{e^{ik_{\nu'}|\vec{r} - \vec{R}_2|}}{|\vec{r} - \vec{R}_2|} \Psi_{\nu'}(\vec{R}), \qquad (7)$$

where $\Psi_{\nu'}(\vec{R})$ is the molecular wave function. The label ν' denotes the quantum state configuration of the molecule, while $\vec{R}$ is the relative internuclear distance ($\vec{R} = \vec{R}_2 - \vec{R}_1$). The first term on the right-hand side (RHS) of Eq. (7) represents an electron with incident momentum $\vec{k}_{\nu_i}$, which is fixed in the $\hat{z}$ direction, plus a molecule in the initial state $\Psi_{\nu_i}(\vec{R})$. The sums in the RHS of this equation are scattering events which leave the molecule in the ν'th final state.

Due to the boundary condition given in Eq. (9) below, only isotropic scattering is described by Eq. (7). This character may be visualized comparing the Eq. (7) above with Eq. (12) of Ref. [38], where the theory for the scattering by a rigid rotor is presented. One may observe that both equations become identical, in the asymptotic limit, if $l' = 0$ in the laboratory frame close-coupling formulation. A second point to observe is that the exact solution of Ostrovsky and Ustimov [23] for the rigid rotor homonuclear scattering problem contains a correction term for the scattering wave function (see Eq. (3.13) of [23]). However, as we show in Sec. II B 3, the ZRP model developed here provides results with similar energy dependence and, once coupled to the adiabatic treatment, it gives similar cross sections as the ones obtained with the exact model, at least for the dimers studied in this work.

The final momentum is calculated through energy conservation,

$$\frac{k_{\nu_i}^2}{2} + E_{\nu_i} = \frac{k_{\nu'}^2}{2} + E_{\nu'}, \qquad (8)$$

where E_{ν_i} and $E_{\nu'}$ are the initial and final molecular energies, respectively. The momentum $k_{\nu'}$ is real for open channels and

imaginary for the closed ones. The ZRP boundary condition, in the multiple-scattering center formulation, becomes

$$\frac{1}{r\psi(\vec{r})} \frac{d[r\psi(\vec{r})]}{dr}\bigg|_{\vec{r} \to \vec{R}_j} = -\kappa_{0j}(k_\nu), \qquad (9)$$

in which $\vec{R}_j$ locates the jth nucleus and $\kappa_{0j}(k_\nu)$ is the parameter for the jth target in the ZRP prescription [Eq. (4)] or the ZRPP one [Eq. (5)]. When applying ZRPP, the argument of κ_0 in the equation above refers to the lower value between k_{ν_i} and k_ν for a given transition [see Eq. (8)]. The reason for such choice is connected to the principle of detailed balance and is discussed in Sec. II B 4. Throughout this article we consider $\nu_i \to \nu$ an excitation process such that $k_\nu < k_{\nu_i}$. In diatomic homonuclear molecules, $\kappa_{0j}(k_\nu)$ is the same for both scattering centers. As discussed before, the van der Waals molecules considered in this work may be modeled by two individual atoms under a nuclear distance constraint. This means that by improving the description of the electron scattering by the single atom, it also improves the electron scattering by the corresponding dimer. This motivates the use of Eq. (5) in the RHS of the boundary condition (9) and it allow us to study the results provided by both ZRP and ZRPP methods.

By inserting Eq. (7) in Eq. (9), and using the orthonormality property of the molecular wave functions, a set of linear equations is obtained for the coefficients $A_\nu^{\nu_i}$ and $B_\nu^{\nu_i}$:

$$A_\nu^{\nu_i}(\kappa_0(k_\nu) + ik_\nu) + \sum_{\nu'} B_{\nu'}^{\nu_i} \langle \nu | \frac{e^{ik_{\nu'}R}}{R} | \nu' \rangle$$

$$= -\langle \nu | e^{i\vec{k}_{\nu_i} \cdot \vec{R}/2} | \nu_i \rangle, \qquad (10)$$

$$B_\nu^{\nu_i}(\kappa_0(k_\nu) + ik_\nu) + \sum_{\nu'} A_{\nu'}^{\nu_i} \langle \nu | \frac{e^{ik_{\nu'}R}}{R} | \nu' \rangle$$

$$= -\langle \nu | e^{-i\vec{k}_{\nu_i} \cdot \vec{R}/2} | \nu_i \rangle, \qquad (11)$$

where the matrix elements are

$$\langle v \mid \frac{e^{ik_{v'}R}}{R} \mid v' \rangle = \int \Psi_v^*(\vec{R}) \frac{e^{ik_v R}}{R} \Psi_{v'}(\vec{R}) R^2 dR d\hat{R}, \qquad (12)$$

$$\langle v | e^{i\vec{k}_{v_i} \cdot \vec{R}/2} | v_i \rangle = \int \Psi_v^*(\vec{R}) e^{i\vec{k}_{v_i} \cdot \vec{R}/2} \Psi_{v_i}(\vec{R}) R^2 dR d\hat{R}. \quad (13)$$

The calculation of such matrix elements depends on the explicit form of the molecular wave functions.

Taking the limit $r \to \infty$ in Eq. (7), the scattering amplitude is obtained:

$$f(\hat{k}') = A_v^{v_i} e^{-ik_v \hat{k}' \cdot \vec{R}_0/2} + B_v^{v_i} e^{ik_v \hat{k}' \cdot \vec{R}_0/2}, \qquad (14)$$

where $\hat{k}'$ is a unit vector describing the direction of the scattered electron. Noting that $k_v R_0 \ll 1$, the cross section for the transition $v_i \to v$ is then calculated using

$$\sigma_{v_i \to v} = \frac{k_v}{k_{v_i}} \int |f(\hat{k}')|^2 d\hat{k}' \approx 4\pi \frac{k_v}{k_{v_i}} |A_v^{v_i} + B_v^{v_i}|^2. \quad (15)$$

1. Elastic cross section in the fixed nuclei approximation

In order to calculate the elastic cross section, the effective molecular wave function product that reduces the matrix elements [Eqs. (12) and (13)] to the fixed nuclei approximation matrix elements is written as

$$\Psi_{v'}(\vec{R}) \Psi_{v_i}^*(\vec{R}) = \frac{\delta(R - R_0)}{R^2} \delta(\hat{R}) \delta_{v' v_i}, \qquad (16)$$

where $\delta(x)$ is the Dirac δ function and $\delta_{\alpha\beta}$ is Kronecker's δ. The Dirac δ functions in Eq. (16) accounts for the fact that in the fixed nuclei approximation, the target does not vibrate nor rotate. Therefore, the molecule remains in its internuclear equilibrium geometry R_0 and in its original space orientation $\hat{R}$. The Kronecker delta translates the physical scenario where excitations associated to the nuclear degrees of freedom are fully disregarded. From energy conservation $k_{v'} = k_{v_i}$.

The calculation of matrix elements given by Eqs. (12) and (13) using (16) are straightforward and the set of Eqs. (10) and (11) becomes trivial. In fact, one obtains two equations for two variables (A and B), which results in

$$A = -\frac{\cos(\vec{k}_{v_i} \cdot \vec{R}_0/2)}{(\kappa_0(k_{v_i}) + ik_{v_i}) + e^{ik_{v_i}R_0}/R_0}$$
$$- i\frac{\sin(\vec{k}_{v_i} \cdot \vec{R}_0/2)}{(\kappa_0(k_{v_i}) + ik_{v_i}) - e^{ik_{v_i}R_0}/R_0}, \qquad (17)$$

and $B = \mathrm{Re}(A) - i\mathrm{Im}(A)$. As one can inspect, the cross section, calculated using Eq. (15), depends on the $\mathrm{Re}(A)^2$ value and, therefore, it is proportional to $\cos^2(\vec{k}_{v_i} \cdot \vec{R}_0/2) \approx 1$, for $k_{v_i}R_0/2 \ll 1$. Analogous development is achieved by taking the average over the molecular orientations. Hence, the cross section is

$$\sigma^{elas}(k_{v_i}) = \frac{16\pi}{(3 - \kappa_0(k_{v_i})R_0)k_{v_i}^2 + (\kappa_0(k_{v_i}) + 1/R_0)^2}. \quad (18)$$

Taking the limit $k_{v_i} \to 0$ in Eq. (18), we immediately recognize the molecular scattering length A_m:

$$A_m = \frac{2R_0}{\frac{R_0}{A} + 1}. \qquad (19)$$

The value of A_m has some interesting implications. Its algebraic sign may be either positive or negative, depending on the value of the electron-atom scattering length A. If $A > 0$, then $A_m > 0$; if $-R_0 < A < 0$, then $A_m < 0$; and if $A < -R_0$, then $A_m > 0$. This last result shows that the composition of two negative electron-atom scattering lengths may provide a positive value for A_m, and, in such a situation, a bound state may exist.

For a better understanding of the cross section's dependence on k_{v_i}, we use Eq. (5) and expand Eq. (18) up to order $k_{v_i}^2$. For sufficiently small momenta,

$$\sigma^{elas}(k_{v_i}) \approx 4\pi A_m^2 \left(1 + \frac{\pi \alpha_d}{3A^2} A_m k_{v_i} + \left[\frac{4\alpha_d \ln k_{v_i}}{3A_m A} + \frac{1}{3}\left(\frac{\pi\alpha_d}{2A^2}\right)^2 \right. \right.$$
$$\left. \left. + \frac{R_0}{2A_m} - 1 \right] A_m^2 k_{v_i}^2 \right). \qquad (20)$$

This equation reduces to the usual ZRP method with a constant parameter κ_0 if the dipole polarizability α_d is set equal to zero. In this case, the elastic cross section depends only on $k_{v_i}^2$. In the same way observed in the electron-atom cross section, Eq. (6), the ZRPP model generates an elastic cross section with a linear dependence on k_{v_i}.

2. Rigid rotor approximation

In the RRA only the rotational degrees of freedom of the molecule are considered. For a diatomic molecule, the rotational wave functions are taken as spherical harmonics $Y_{JM}(\hat{R})$, J and M being the rotational quantum numbers (see Chap. 9 of [39]). In this case, the effective molecular wave-function product is written as

$$\Psi_{v=JM}(\vec{R}) \Psi_{v'=J'M'}^*(\vec{R}) = \frac{\delta(R - R_0)}{R^2} Y_{JM}(\hat{R}) Y_{J'M'}^*(\hat{R}). \qquad (21)$$

In such an approximation, the target may be excited to another rotational quantum level: $v_i = J_i M_i \to v = JM$. Setting the initial rotational state of the molecule as the ground state ($J_i = 0$, $M_i = 0$), the matrix element (13) is calculated making use of the standard plane-wave expansion in spherical coordinates:

$$\langle JM | e^{i\vec{k}_{J_i} \cdot \vec{R}/2} | 00 \rangle = \sqrt{4\pi} i^J j_J\left(\frac{k_{J_i} R_0}{2}\right) Y_{JM}^*(\hat{k}_{J_i}), \quad (22)$$

where $j_a(x)$ are the spherical Bessel functions of order a. The matrix element of Eq. (12) is easily obtained using the orthonormality property of the spherical harmonics:

$$\langle JM | \frac{e^{ik_{J'}R}}{R} | J'M' \rangle = \frac{e^{ik_{J'}R_0}}{R_0} \delta_{J'J} \delta_{M'M}. \qquad (23)$$

The deltas present in Eq. (23) get rid of the sums present in the set of linear equations (10) and (11). In such situation, analogous to what happened in the fixed nuclei case, we obtain two sets of equations for two variables ($A_{JM}^{J_i M_i}$ and $B_{JM}^{J_i M_i}$), which couple the rotational quantum numbers J_i, M_i and J, M. Taking the average on the initial rotational projections

M_i and summing over M in Eq. (15), we obtain

$$\sigma_{J_i \to J}(k_{J_i}) = \sigma_{0 \to J}(k_{J_i}) \sum_{L=J-J_i}^{J+J_i} \left[\left(\frac{k_{J_i} R}{2} \right)^{(L-J)} \right.$$
$$\left. \times \frac{(2J+1)!! \langle J0J_i0|L0 \rangle}{(2L+1)!!} \right]^2, \qquad (24)$$

where $\langle J_1 M_1 J_2 M_2 | J M \rangle$ are Clebsch-Gordan coefficients and, for small momenta, the $0 \to J$ cross section is

$$\sigma_{0 \to J}(k_0) = \frac{k_J}{k_0} \left[\frac{(k_0 R_0)^J}{2^J(2J+1)!!} \right]^2$$
$$\times \frac{16\pi(2J+1)}{(3 - \kappa_0(k_J)R_0)k_J^2 + (\kappa_0(k_J) + 1/R_0)^2}. \quad (25)$$

From selection rules, only even values of J are allowed in the equation above. One may notice that for $J = 0$ the elastic cross section in Eq. (18) is recovered.

3. Comparison with other rigid rotor models

In this section we compare our results to similar ones that can be accessed with other formulations found in literature for the scattering of a particle by a rigid rotor. More specifically, we pay attention to the exact solution presented by Ostrovsky and Ustimov [23] and the more familiar adiabatic approximation. In the past, Drukarev and Yurova [22] studied the rovibrational excitation of ordinary diatomic molecules by electron impact by applying the adiabatic approximation to the ZRP scattering amplitude.

The adiabatic scattering amplitude is calculated using [22]

$$f_{J_i M_i \to J M}^{(AD)}(\vec{k}_{\nu_i}, \vec{k}_\nu) = \int Y_{JM}^*(\hat{R}) f(\vec{k}_{\nu_i}, \vec{k}_\nu, \vec{R}) Y_{J_i M_i}(\hat{R}) d\hat{R}, \qquad (26)$$

where $f(\vec{k}_{\nu_i}, \vec{k}_\nu, \vec{R})$ is the fixed nuclei ZRP scattering amplitude.

Inserting Eq. (14) into Eq. (26), and considering coefficients A and B as given by Eq. (17), we find

$$\sigma_{J_i \to J}^X(k_{J_i}) = 16\pi \frac{k_J}{k_{J_i}}(2J+1)$$
$$\times \sum_{l=0}^{\infty} \sum_{L=|l-J_i|}^{l+J_i} \sum_{l'=|L-J|}^{L+J} \left| \frac{j_l(k_{J_i}R_0/2) j_{l'}(k_J R_0/2)}{\kappa_0 + \beta_{Ll}^X} \right|^2$$
$$\times \frac{(2l+1)(2l'+1)}{2L+1} \langle J0l'0|L0 \rangle^2 \langle J_i0l0|L0 \rangle^2. \qquad (27)$$

One may recognize that the same expression for the rotational transition cross section is provided by the exact model [23]. The main difference between them is found in the β factor and, for this reason, we attach a label X to it. In what follows

X=EX refers to the exact solution, while X=AD to the adiabatic one.

For the adiabatic approximation, one obtains

$$\beta_{Ll}^{AD} = ik_J + (-1)^l \frac{e^{ik_J R_0}}{R_0}. \qquad (28)$$

Within the exact model, Ostrovsky and Ustimov [23] calculated a correction factor given by

$$\beta_{Ll}^{EX} = \beta_{Ll}^{AD} + 2i \sum_{m>0}^{\infty} \sum_{n=|L-m|}^{L+m} \frac{(2n+1)(2m+1)}{2L+1}$$
$$\times \langle m0n0|L0 \rangle^2 \left(1 + \frac{2m_e}{\mu} \right)$$
$$\times \left[k_m j_n \left(\frac{k_m R_0}{2} \right) h_n^{(1)} \left(\frac{k_m R_0}{2} \right) \right.$$
$$\left. - k_{J_i} j_n \left(\frac{k_{J_i} R_0}{2} \right) h_n^{(1)} \left(\frac{k_{J_i} R_0}{2} \right) \right], \qquad (29)$$

where the index m respects the parity of the initial rotational quantum number J_i and the index n runs over the integers of parity $L + J_i$. The $h_n^{(1)}(x)$ stands for the spherical Hankel function of the first kind. We may consider $(1 + 2m_e/\mu) \approx 1$, since the electron mass m_e is much smaller than the mass of the rigid rotor μ. Such an equation reveals that if $k_m/k_J \approx 1$, the exact solution becomes identical to the adiabatic approximation.

The values of the rotational constants are small for the dimers studied in this work, as one can notice in Table IV. Due to this, the differences between β_{Ll}^{AD} and the leading order of β_{Ll}^{EX} become prominent in the very-low-energy regime ($E < 0.1$ meV). The most important feature provided by the exact model, when compared to the adiabatic one, is that a rotational resonance exists if the condition $\kappa_0 = \text{Re}(\beta_{Ll}^{EX})$ is obeyed. Nevertheless, as discussed in [23], this condition is only fulfilled if the electron-atom scattering length A is very close to the equilibrium position R_0 of the homonuclear molecule. This makes the rotational resonance behavior unlikely, and, in fact, it is not observed for the rare-gas dimers, according to our work.

In order to compare the RRA proposed in this article to the adiabatic one, we consider $J_i = 0$ in Eq. (27):

$$\sigma_{0 \to J}^{AD}(k_0) = 16\pi \frac{k_J}{k_0}(2J+1)$$
$$\times \sum_{l=0}^{\infty} \sum_{l'=|l-J|}^{l+J} \left| \frac{j_l(k_0 R_0/2) j_{l'}(k_J R_0/2)}{\kappa_0(k_J) + \beta_{ll}^{AD}} \right|^2$$
$$\times (2l'+1) \langle J0l'0|l0 \rangle^2, \qquad (30)$$

where we assumed that the κ_0 parameter may depend on the electron momentum. Noticing that $k_J R_0 \approx k_0 R_0 \ll 1$, and, for $x \ll 1$, $j_a^2(x) \gg j_b^2(x)$ for any $b > a$, we obtain

$$\sigma_{0 \to J}^{AD}(k_0) \approx \sigma_{0 \to J}(k_0) g_{0J}, \qquad (31)$$

where $\sigma_{0 \to J}(k_0)$ is given by Eq. (25), and

$$g_{0J} = \sum_{l=0}^{J} \left[\frac{\sqrt{2(J-l)+1}(2J+1)!! \langle J0(J-l)0|l0 \rangle (R_0+A)}{(2l+1)!!(2[J-l]+1)!!(R_0+(-1)^l A)} \right]^2. \qquad (32)$$

Equations (31) and (32) reveal that the rotational transition cross sections [Eq. (25)], based on an approximated wave function [Eq. (7)], furnish results smaller in magnitude but with a similar dependence on the incident electron momentum when compared to the adiabatic model. The term g_{0J} [Eq. (32)] works as a scale factor and, as we can see, it does not depend on the electron energy in the energy range studied in this work. It comes from the fact that, in the adiabatic approximation, partial waves beyond the spherical wave are taken into account in the scattering wave function. Table I brings the numerical values for g_{0J} for the rare-gas dimers.

Figure 2 presents results to the $0 \to 2$ rotational cross section regarding the Ar_2 dimer. A crucial point is that the exact model (squares) provides results alike to the adiabatic model (triangles). Since this feature is observed for all dimers studied, we find out that the correction factor β_{Ll}^{EX} calculated by Ostrovsky and Ustimov [23], presented in Eq. (29), is small and its impact in the final cross section is unnoticeable, at least for the scattering of electrons by rare-gas dimers case. The results obtained with our model (dashed line), Eq. (25), are, as discussed in this section, smaller in magnitude with respect to the exact and adiabatic models. Notwithstanding, Eq. (25) combined with the scale factor g_{02}, calculated through Eq. (32), gives outcomes (full line) in good agreement with both exact and adiabatic models.

4. Considerations regarding the principle of detailed balance

The principle of detailed balance (PDB) establishes a well-defined relation between excitation and deexcitation cross sections for given initial and final states. Mathematically, it is embodied in the T matrix for a given $a \leftrightarrow b$ transition. The relation between the excitation and deexcitation cross sections is obtained fixing $T_{a \to b} = T_{b \to a}$. Physically, it translates the microscopical reversibility of physical reactions (see Chap. 16 of [40]). Its relevance for practical applications lies in the fact that the deexcitation cross sections can be readily obtained by the PDB, instead of repeating a laborious calculation from the theory.

In this section the PDB is analyzed in the context to the RRA. It is so chosen because it permits a straightforward

comparison to the theory of scattering by a rigid rotor of Arthurs and Dalgarno [38]. From this reference, we find that if the PDB is rigorously respected, the following relation holds:

$$k_{J_i}^2(2J_i+1)\sigma_{J_i \to J} = k_J^2(2J+1)\sigma_{J \to J_i}. \qquad (33)$$

Within the ZRPP prescription, by taking Eq. (25) for the $0 \to J$ transition and considering the respective cross section for the $J \to 0$ process, we obtain

$$k_0^2 \sigma_{0 \to J} = (2J+1)k_J^2 \sigma_{J \to 0} f(k_0, k_J), \qquad (34)$$

where

$$f(k_0, k_J) = \left(\frac{k_0}{k_J} \right)^{2J} \frac{(3-\kappa_0(k_J)R_0)k_J^2+(\kappa_0(k_J)+1/R_0)^2}{(3-\kappa_0(k_J)R_0)k_0^2+(\kappa_0(k_J)+1/R_0)^2}. \qquad (35)$$

In order for the principle of detailed balance to be strictly obeyed we should have that $f(k_0, k_J) = 1$. Analyzing Eq. (35) we are led to conclude that the PDB is not respected in both ZRP and ZRPP models, since in any inelastic transition we necessarily have $k_J \neq k_0$. Working in a more flexible scenario, we find that the PDB is numerically respected as long as $k_0 \approx k_J$, a situation which is found for energies far from the rotational thresholds.

If the PDB does not hold in the ZRPP model, it sounds reasonable to investigate how it behaves in the adiabatic model. In this model, the explicit expressions
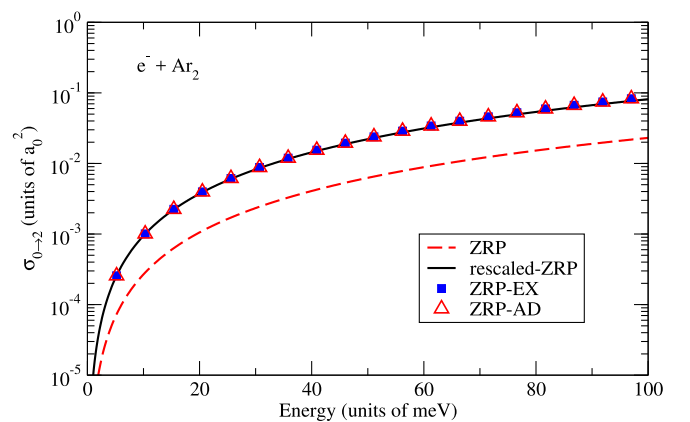

FIG. 2. Rotational $0 \to 2$ cross section for Ar_2 with the parameters given in Tables III and IV. Legends are as follows: Dashed line is the results provided by the model of this work [Eq. (25)], which we call ZRP; full line is the ZRP results multiplied by the scale factor g_{02} present in Table I, this model is called "rescaled-ZRP"; the triangles are the results from the adiabatic model, called ZRP-AD; squares are results given by the exact model of Ostrovsky and Ustimov [23], called ZRP-EX.

TABLE I. Numerical values of g_{0J} for $J=2$ (first line) and $J=4$ (second line) for the rare-gas dimers. The parameters used in Eq. (32) are presented in Tables III and IV. The values for Xe_2 were calculated with $A=-5.13$ and $A=-6.09$, respectively.

	He_2	Ne_2	Ar_2	Kr_2	Xe_2
g_{02}	9.90	5.83	3.53	2.60	2.18/2.07
g_{04}	84.0	54.8	38.2	31.5	28.5/27.6

obtained are

$$\sigma_{0\to J}^{AD} = 16\pi \frac{k_J}{k_0} \sum_{l=0}^{\infty} \sum_{l'=0}^{\infty} \frac{j_l^2(k_0 R_0/2) j_{l'}^{\prime 2}(k_J R_0/2)(2l+1)(2l'+1)\langle l0l'0|J0\rangle^2}{k_J^2[1+(-1)^l(2-\kappa_0(k_J)R_0)]+(\kappa_0(k_J)+(-1)^l/R_0)2}, \tag{36}$$

$$\sigma_{J\to 0}^{AD} = \frac{16\pi k_0}{(2J+1)k_J} \sum_{l=0}^{\infty} \sum_{l'=0}^{\infty} \frac{j_{l'}^{\prime 2}(k_0 R_0/2) j_l^2(k_J R_0/2)(2l+1)(2l'+1)\langle l0l'0|J0\rangle^2}{k_0^2[1+(-1)^{l'}(2-\kappa_0(k_J)R_0)]+(\kappa_0(k_J)+(-1)^{l'}/R_0)^2}. \tag{37}$$

Comparing both equations, we are led to conclude that the PDB is satisfied if

$$k_J^2[1+(-1)^l(2-\kappa_0(k_J)R_0)]+(\kappa_0(k_J)+(-1)^l/R_0)^2$$
$$= k_0^2[1+(-1)^l(2-\kappa_0(k_J)R_0)]+(\kappa_0(k_J)+(-1)^l/R_0)^2. \tag{38}$$

As ascertained in the analysis for the ZRP and ZRPP models, the PDB is numerically respected for energies far from the threshold ($k_0 \approx k_J$).

The adiabatic prescription, on the other side, offer us another interesting point of view. In the physical scenario where $k_J \neq k_0$, we find that $k_J, k_0 \ll 1$ such that k_J^n and k_0^n are practically equal to zero for $n \geqslant 2$. Due to that, the first terms in the left-hand side and right-hand side of Eq. (38) are negligible for the rare-gas dimers. Then, we find why it is interesting to choose to work with the lower value between k_J and k_0 for the argument of the κ_0 parameter [as discussed above Eq. (9)]: such a prescription enhances the agreement between the ZRP and ZRPP models for energies closer to the threshold and improves the application of the numerical version of the PDB in the AD model.

As an illustrative example of the previous discussion, we present in Fig. 3 the deexcitation cross section of the $2 \to 0$
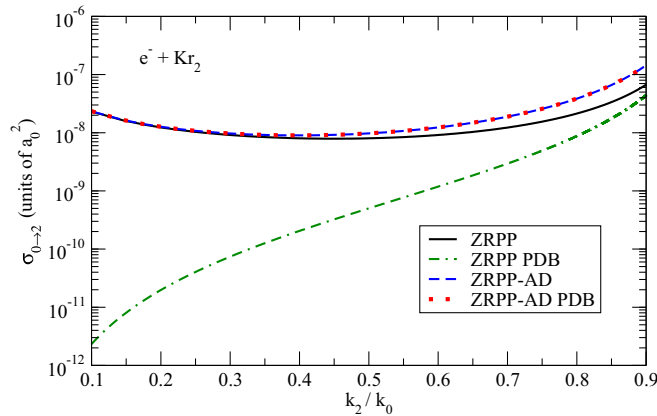

FIG. 3. Deexcitation cross section for the $2 \to 0$ transition for electron-Kr_2 computed from the ZRPP compared to those provided by the principle of detailed balance (PDB) for very low electron momenta (where $k_2 \neq k_0$). Solid line: ZRPP cross section; double-dashed-dotted line: ZRPP calculated using the PDB relation [Eq. (33)]; dashed line: ZRPP + AD (adiabatic approximation) cross section; dotted line: ZRPP+AD calculated using the PDB relation [Eq. (33)]. For the sake of completeness, the energy range covered in this figure goes from $\sim 2.0 \times 10^{-4}$ meV ($k_2/k_0 = 0.1$) to ~ 0.08 meV ($k_2/k_0 = 0.9$).

transition for electron-Kr_2. Only the very-low-electron-momenta range is considered (where $k_2 \neq k_0$). We perceive that the ZRPP (solid line) cross section is strongly different from that obtained from the PDB (double-dashed-dotted line), as predicted by Eqs. (34) and (35). As stated above, when the adiabatic approximation is regarded, the deexcitation cross sections computed by the pure method or from the PDB become indistinguishable (see dashed and dotted lines in the figure).

The failure of the ZRP model to respect the strict form of the PDB can also be seen as a consequence of the fact that only spherical waves are produced in the final scattering channel. The improvement in the PDB, observed when the cross sections are computed in the adiabatic approach, comes from the fact that the partial waves present in the exponentials of Eq. (14) are no longer neglected.

5. Short-range versus long-range effects

It is known that rotational excitation of homonuclear molecules by low-energy electrons is often well modeled by the long-range electron interaction with the quadrupole moment of the molecule. The theory that recognizedly deals with this hypothesis is described in the Gerjuoy-Stein (GS) article [41]. In this approach, the rotational excitation cross section is given by

$$\sigma_{J\to J+2}^{GS} = \frac{k_{J+2}}{k_J} \frac{8\pi}{15} Q^2 \frac{(J+2)(J+1)}{(2J+3)(2J+1)}, \tag{39}$$

which strongly depends on the magnitude of the molecular quadrupole moment Q.

In order to compare the GS model (long-range quadrupole) to the ZRP models (short-range effects), we have taken the numerical value for the quadrupole moment Q of each rare-gas dimer, except Xe_2, from the *ab initio* calculation (MP2) of Ref. [42]. For Xe_2 the Q value was calculated with the GAMESS software [43] using the basis set aug-cc-pVTZ [44]. This basis set was chosen inspired in the theoretical article devoted to the study of the interaction potential between the atoms that form the respective dimer. The quadrupole values are listed in Table II.

From the values of Table II, one can notice that, from He_2 to Kr_2, the long-range quadrupole potential, given by the

TABLE II. Quadrupole moments for the dimers in atomic units. All values are taken from [42], except Xe_2, as discussed in the text.

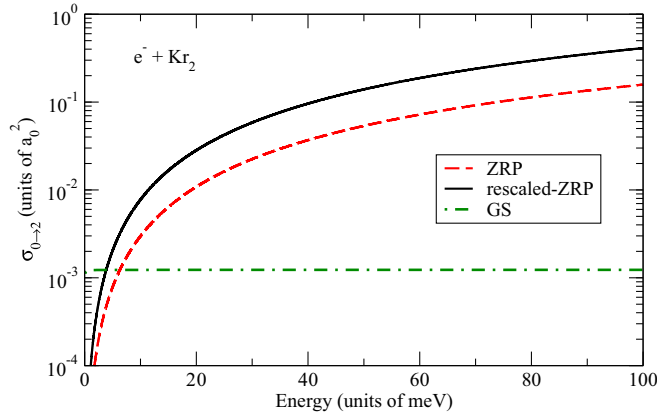|	He_2	Ne_2	Ar_2	Kr_2	Xe_2
Q	−0.0012	−0.0022	−0.0186	−0.0332	16.67

FIG. 4. Rotational excitation cross section for $0 \to 2$ transition in electron-Kr$_2$ scattering. Dashed line: ZRP cross section [Eq. (25)]; solid line: rescaled-ZRP [Eq. (25) combined with Eq. (32)]; dashed-dotted line: Gerjuoy-Stein model (GS) [Eq. (39)]. All results were obtained in the RRA, and the parameters used are in Table II for the GS and Tables III and IV for the ZRP.

asymptotic expression $V \to Q P_2(\cos\theta)/r^3$, is weak when compared to the respective quantity in typical diatomics like H$_2$ ($Q \approx 0.5$ a.u.) and N$_2$ ($Q \approx -1.0$ a.u.).

In Fig. 4 we show the cross section provided by the GS model compared to the ZRP and rescaled-ZRP for the Kr$_2$ dimer. Due to the value of the quadrupole moment of Kr$_2$, the GS cross section is significantly smaller than those provided by the ZRP models (except for energies very close to the threshold). It strongly suggests that, in spite of the existence of the long-range quadrupole effect, the short-range potential may be the dominant mechanism for the rotational excitation dynamics in electron-rare-gas dimers. Similar results as the ones reported in Fig. 4 are found for He$_2$, Ne$_2$, and Ar$_2$. Clearly, Xe$_2$ can be an exception to the statement above, once its Q value is much larger than the others, but we still report the results for this system for future reference in related investigations.

6. Rovibrational model

The inclusion of the vibrational states of the molecule is very important in order to properly describe the phenomenology of the scattering process. The RRA, for example, fails to respect the uncertainty principle, once the zero-point energy associated to the nuclear vibrational motion is not taken into account. The molecular wave function, with both vibrational and rotational degrees of freedom, is written as

$$\Psi_{v=nJM}(\vec{R}) = \frac{\Phi_n(R)}{R} Y_{JM}(\hat{R}). \quad (40)$$

As a preliminary application of ZRP to the electron-dimer scattering problem, we consider the vibrational states of the molecule in the harmonic approximation, such that $\Phi_n(R)$ are the solutions of the quantum harmonic oscillator. It is assumed that the molecule is in its vibrational ground state in the initial scattering state.

TABLE III. Parameters for the noble gas atoms. The scattering length A is given in units of a_0 and the dipole polarizability α_d is reported in units of a_0^3. The scattering lengths are taken from beam experiments. For He and Ne, they are taken from the work of Shigemura *et al.* [34]; for Ar, Kr, and Xe the values of A are taken from the experiment of Kurokawa *et al.* [35]. For Xe, we also considered the scattering length reported in the swarm experiment of Hunter *et al.* [45]. All the atomic polarizabilities were taken from the article of Miller and Benderson [46].

	He	Ne	Ar	Kr	Xe
A	1.194[a]	0.206[a]	-1.365[b]	-3.06[b]	-5.13[b]/-6.09[c]
α_d	1.383	2.67	11.1	16.8	27.3

[a]Beam experiment Ref. [34].
[b]Beam experiment Ref. [35].
[c]Swarm experiment Ref. [45].

The matrix element (12) for such a molecular wave function becomes

$$\langle v | \frac{e^{ik_{v'}R}}{R} | v' \rangle = \langle n | \frac{e^{ik_{n'J}R}}{R} | n' \rangle \delta_{J'J} \delta_{M'M}. \quad (41)$$

Observe that the RHS of Eq. (41) depends only on the molecular vibrational wave functions. Such a matrix element is provided in leading order by Gribakin [24] and, for the sake of completeness, is presented in Appendix.

The matrix element (13) becomes an integral which depends on the internuclear distance and the spatial orientation. The analytical development is shown in Appendix. It is important to notice that the coupling of the vibrational and rotational states of the molecule is incorporated in this matrix element.

The cross section is calculated through Eq. (15), setting $v_i = |0 J_i M_i\rangle \to v = |n J M\rangle$, averaging over M_i, and summing over M. In the RVA, we were not able to obtain analytical expressions for the cross sections, as it was done in the prior approximations. This is a consequence of the sum over the vibrational states n', which formally goes from $n' = 0$ to $n' \to \infty$. For numerical calculation purposes, the sum must be truncated at $n'_{\max}$. We fixed $n'_{\max} = 20$, because we verified that the value of the coefficients $A_{nJM}^{0 J_i M_i}$ and $B_{nJM}^{0 J_i M_i}$ are practically equal to zero. If we take $n'_{\max} \equiv 0$, the RVA is reduced to the RRA as expected. From Eq. (10), the final electron momentum, considering the harmonic potential approximation for the vibrational wave function, is

$$k_{nJ} = \sqrt{k_{0J_i}^2 - 2n\omega_v - 2B_r[J(J-1) - J_i(J_i-1)]}, \quad (42)$$

where ω_v and B_r are the vibrational and rotational constants, respectively.

III. PARAMETERS OF THE MODEL

In this section, we present the parameters required for the calculation of elastic and rovibrational cross sections. Regarding the noble gas atoms, there are two parameters that must be known to calculate the $\kappa_0(k_v)$ as in Eq. (5): the electron-atom scattering length A and the atomic dipole polarizability α_d. These are shown in Table III.

Concerning the dimer molecules, there are three molecular parameters required by the model. These are the reduced

TABLE IV. van der Waals dimer parameters in atomic units: reduced mass $\mu/10^3$; equilibrium position R_0, taken from Cybulski and Toczylowski [10] for He_2 and Ne_2, from Haley and Cybulski [47] for Ar_2 and Kr_2, and from Jerabek *et al.* [48] for Xe_2; vibrational constant $\omega_v/10^{-5}$, calculated through potential fittings [see Eqs. (43) and (44)]; and rotational constants $B_r/10^{-7}$.

	$\mu/10^3$	R_0	$\omega_v/10^{-5}$	$B_r/10^{-7}$
He_2	3.67	5.62[a]	14.86	43.3
Ne_2	18.4	5.86[a]	12.97	7.93
Ar_2	33.0	7.10[b]	14.73	3.00
Kr_2	76.4	7.60[b]	10.74	1.14
Xe_2	99.1	8.24[c]	10.40	0.731

[a]Reference [10].
[b]Reference [47].
[c]Reference [48].

mass μ, the equilibrium internuclear distance R_0, and the vibrational constant ω_v. The rotational constant B_r is also required, but it can be calculated using the reduced mass and equilibrium configuration through the relation $B_r = 1/2\mu R_0^2$. All the molecular parameters are presented in Table IV.

Since the harmonic approximation is used throughout this paper, the vibrational constant is calculated by $\omega_v = \sqrt{U''(R_0)/\mu}$, where the potential was represented for all dimers, except for Xe_2, by the fitting [10,47]

$$U(R) = A_p e^{-\alpha R + \beta R^2} + \sum_{n=3}^{8} f_{2n}(R, b) \frac{C_{2n}}{R^{2n}}. \quad (43)$$

For Xe_2, the following fitting used was [48]:

$$U(R) = e^{-\alpha R} \sum_{p=-1}^{3} A_p R^p + \sum_{n=3}^{8} f_{2n}(R, b) \frac{C_{2n}}{R^{2n}}, \quad (44)$$
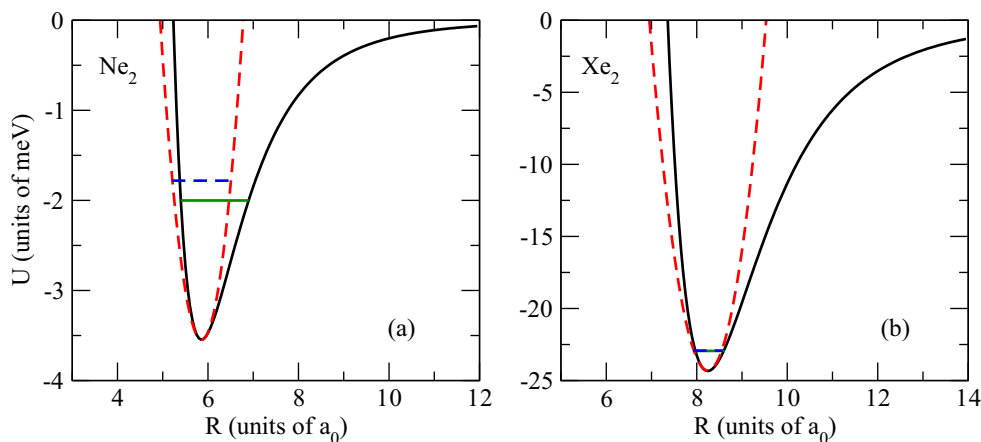
TABLE V. Electron-molecule scattering lengths A_m in atomic units, calculated by Eq. (19) for all rare-gas dimers.

	He_2	Ne_2	Ar_2	Kr_2	Xe_2
A_m	1.97	0.398	−3.38	−10.24	−27.18/−46.68

where A_p, α, β, and b are adjustable parameters, C_{2n} are the dispersion coefficients, and $f_{2n}(R, b)$ is the damping function,

$$f_{2n}(R, b) = 1 - e^{-bR} \sum_{k=0}^{2n} \frac{(bR)^k}{k!}. \quad (45)$$

The fitting parameters and the dispersion coefficients can be found in the respective references.

The He_2 dimer configures a special case since its potential is very shallow, and some *ab initio* potentials are not even deep enough to support a bound vibrational state [10]. More accurate potentials [11], nonetheless, reveal that a vibrational state is possible, and the zero-point energy is very close to the dissociation threshold ($D_e \approx 10^{-4}$ meV). This fact leads to only one rovibrational bound state possible for such dimer [49], and, therefore, the calculation of rovibrational excitation cross sections would not make any sense. For Ne_2, two vibrational bound states are found [10]. For this reason, only the transitions $n_i = 0 \rightarrow n = 1$ and $J_i = 0 \rightarrow J = 2$ are considered. For the remaining dimers, Ar_2, Kr_2, and Xe_2, the potentials support several rovibrational bound states [47,48].

For illustrating purposes, Fig. 5 shows the potential surfaces fitted from Eq. (43) for Ne_2 and Eq. (44) for Xe_2, compared to its harmonic potential approximation. The zero-point energies calculated for both potentials are also shown. For Ne_2, such energy in harmonic approximation is larger than the reference value, but it still works as a reasonable approximation. For Xe_2, on the other hand, the zero-point energy is nearly the same for both potentials. Given the atomic and molecular parameters, we then proceed to analyze the results obtained within this model.
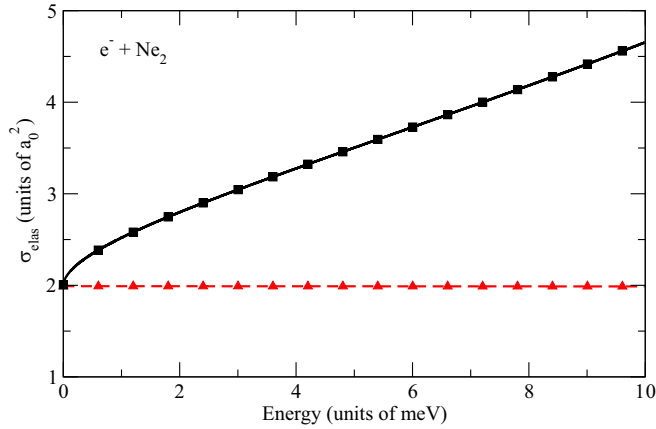

FIG. 5. Panel (a): solid line is Ne_2 potential fitting; horizontal solid line represents the zero-point energy; dashed line is the Ne_2 harmonic potential approximation; horizontal dashed line represents the zero-point energy in harmonic potential approximation. Panel (b): same as panel (a), but for Xe_2.

FIG. 6. Elastic cross section for $e^- + Ne_2$ calculated in the RVA. The results provided by fixed nuclei and RRA furnish similar results. Dashed line with triangles: ZRP model; solid line with squares: ZRPP model.
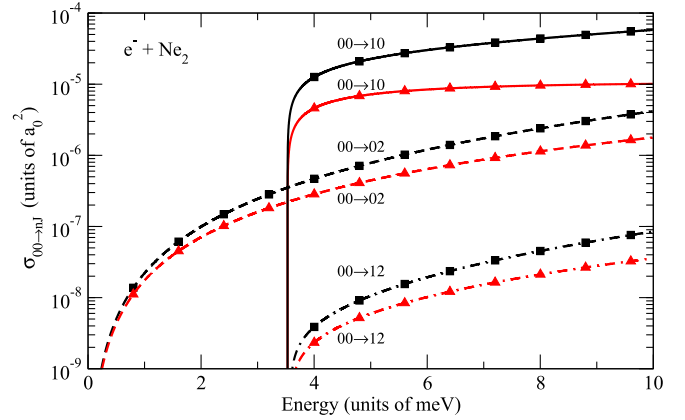

FIG. 7. Excitation cross sections for $e^- + Ne_2$. Solid line with triangles and solid line with squares are the results for vibrational excitation $00 \rightarrow 10$ cross section provided by ZRP and ZRPP models, respectively. Dashed line with triangles and dashed line with squares are the results for rotational excitation $00 \rightarrow 02$ cross section provided by ZRP and ZRPP models, respectively. Dashed-dot line with triangles and dashed line with squares are the results for rovibrational excitation $00 \rightarrow 12$ cross section provided by ZRP and ZRPP models, respectively.

IV. GENERAL RESULTS FOR ELASTIC, ROTATIONAL, AND ROVIBRATIONAL TRANSITIONS

Results for argon dimer were reported to compare those produced by the ZRP and ZRP rescaled to the exact solution of Ostrovsky and Ustimov [23], and the adiabatic approximation in the RRA in Sec. II B 3. Meanwhile, the krypton dimer was considered to discuss the connection between the ZRP and the principle of detailed balance (see Sec. II B 4). We also used this system to compare the ZRP results with those provided by the long-range quadrupolar model of Gerjuoy-Stein [41].

In this section, we present results for elastic, rotational, and rovibrational transitions for selected dimers. We have chosen Ne_2 and Xe_2 as representative systems to illustrate the results provided by the ZRP and the ZRPP prescriptions. Argon, krypton, and xenon have negative electron-atom scattering lengths (see Table III). For this reason, we decided to report and to discuss mainly the xenon atom. Another motivation to focus on Xe_2 among others is the discrepancy of the electron-atom scattering length reported in literature. This also occurs for other dimers but is not as considerable as in the Xe case. Finally, in Sec. IV C, the mass of the krypton dimer was varied in order to visualize how the oscillator mass affects the vibrational cross sections.

Table V brings the electron-molecule scattering lengths A_m for all dimers calculated by Eq. (19). Although such values are calculated by a simple equation which is a consequence of the ZRP approximation, we believe these would be close to the ones provided by an *ab initio* method or an experiment, if possible.

A. Electron – Neon dimer

Figure 6 shows the elastic cross section for $e^- + Ne_2$ in the RVA, considering the ZRP and ZRPP prescriptions. The inclusion of the polarizability term rises the elastic cross section, while the result in the pure ZRP is flat (as also observed for $e^- + He_2$, not shown here). This may be understood through Eq. (20), which shows that the cross section depends on k_{v_i} when the polarizability α_d is considered. Similar results are

obtained in the fixed nuclei approximation and RRA. The fact that Ne atom has a positive scattering length makes the linear term in k_{v_i} always positive and, hence, the contribution to the cross section is also always positive. Such behavior is also seen in the elastic cross section for electron-Ne atoms [34] for small energies. This is no coincidence once there is a similarity between the linear term in molecular [Eq. (20)] and atomic cross-section expansion [Eq. (6)].

Figure 7 presents the vibrational $00 \rightarrow 10$ (solid line), the rotational $00 \rightarrow 02$ (dashed line), and the rovibrational $00 \rightarrow 12$ cross sections. As observed in the elastic transition (see Fig. 6), the vibrational and rotational excitation cross sections rise faster with energy when polarizability terms are considered in expansion (5). Nonetheless, the vibrational cross section is more sensitive to the polarizability term, once a saturation is seen for ZRP results of about 6 meV, and such behavior does not happen in ZRPP results in the reported energies. As we can see, the rovibrational cross section is identical to the rotational one, except for being shifted toward higher energies and with smaller magnitude.

One could notice that the vibrational excitation energy does not exceed ~ 2 meV if the true anharmonic potential is considered, while this energy is greater than 3 meV in the harmonic approximation. These issues may affect the validity of the results for this dimer. The level of reliability of the harmonic approximation remains as a point for further investigations, and we presented the results here for future reference in related works.

B. Electron – Xenon dimer

The results for the elastic cross sections of Xe_2 are presented in Fig. 8. Due to a discrepancy in the electron-atom scattering length given by Kurokawa *et al.* [35] and Hunter *et al.* [45], we have calculated the cross sections for both
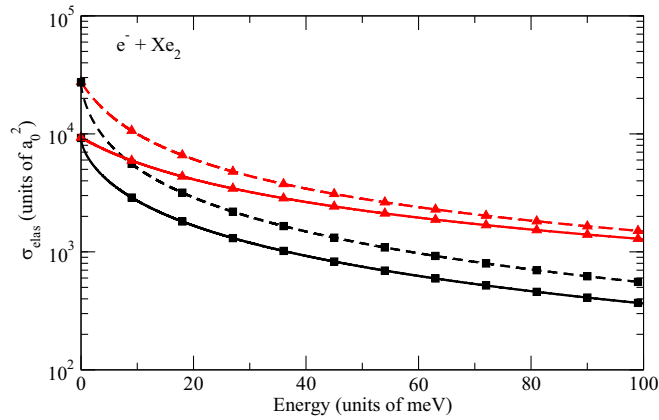
FIG. 8. Elastic cross section for $e^- + Xe_2$ within the RVA. Solid line with triangles and solid line with squares are results provided by ZRP and ZRPP models considering Kurokawa *et al.* electron-atom scattering length $A = -5.13$ [35]. Dashed line with triangles and dashed line with squares are results provided by ZRP and ZRPP models considering Hunter *et al.* electron-atom scattering length $A = -6.09$ [45].

values in order to visualize how these vary with such parameters. We see that the elastic cross section is sensitive to the value of A, especially for energies below 10 meV. To understand this, one may look to Eq. (19). From this, we conclude that when the electron-atom scattering length is negative and its absolute value gets closer to the equilibrium position, the magnitude of the electron-molecule scattering length A_m increases rapidly. This is the case of Xe_2 once the reported values for A are $-5.13 \, a_0$ and $-6.09 a_0$, which provides A_m of $-27.18 \, a_0$ and $-46.68 \, a_0$, respectively, as we can see in Table V.

Figure 8 also shows that the inclusion of the polarization terms makes the elastic cross section decrease in magnitude when compared to the results for constant κ_0. This is expected, since the linear term in k_{v_i} in Eq. (20) is negative, which is a consequence of negative values of electron-molecule scattering length. The same behavior is also observed for Ar_2 and Kr_2 when the polarizability is considered.

In Fig. 9 the vibrational $00 \rightarrow 10$, the rotational $00 \rightarrow 02$, and the rovibrational $00 \rightarrow 12$ excitation cross sections are shown for both reported electron-atom scattering lengths. As shown in Fig. 9, the cross sections provided by the ZRPP model are always lower than the ZRP model, as noticed in the elastic cross-section behavior. The greatest difference between the results for different scattering lengths is seen in the $00 \rightarrow 10$ transition, mainly in energies closer to the threshold.

The rovibrational transition $00 \rightarrow 12$ cross section is shown to be small when compared to others, as also seen in Ne_2 (see Fig. 7). These results suggest that the probability of the target to suffer a rovibrational excitation is lower than the probability of suffering a pure vibrational or a pure rotational excitation.

C. Rotational and rovibrational models compared

An advantage of our model is that it allows us to study how the cross sections depend on the molecular parameters. From Eq. (18), for example, we realize that the elastic cross section does not depend on the mass of the dimer at all. On the other hand, Eq. (25) reveals that the rotational transition cross section has a nonexplicit dependence on the mass of the rigid rotor in k_J, once the rotational constant varies with the dimer mass. The impact of such dependence in the cross section is mainly in the position in which the rotational channel opens. Far from the threshold, nevertheless, the rotational cross section is insensitive to the mass, since $k_J \approx k_0$. Figure 10 presents cross sections for the vibrational transition $00 \rightarrow 10$ in the ZRP model considering several masses for the Kr_2 dimer (the mass values used are indicated in the figure). As the vibrational constant ω_v depends on the mass (see Sec. III), the position where the vibrational channel opens is different for each mass value. Differently from the rotational case, the mass of the dimer has an expressive impact in the vibrational transition cross section, as one may observe in Fig. 10. These results may be understood through the matrix elements calculated in the Appendix, where we notice that Eqs. (A2) and (A16) explicitly depend on the mass of the dimer μ, and, owing to that, the vibrational transition cross section also presents a dependence on the μ parameter. Figure 10 shows that the smaller the value of
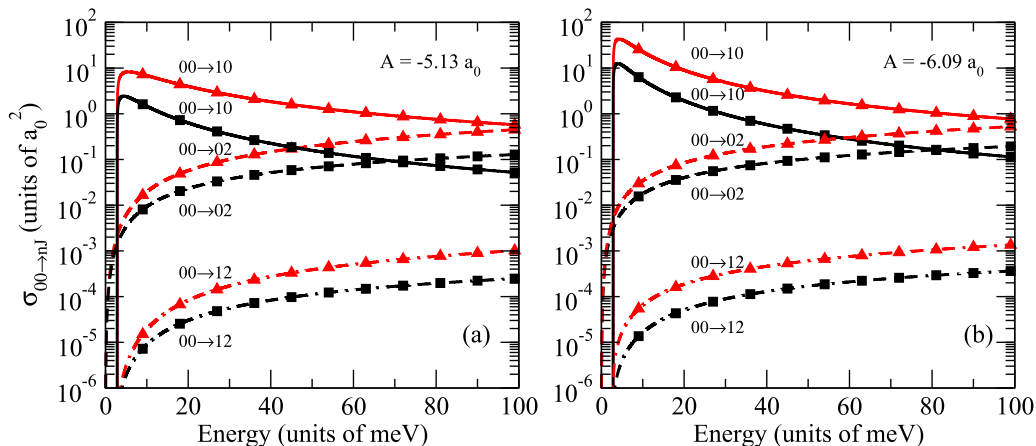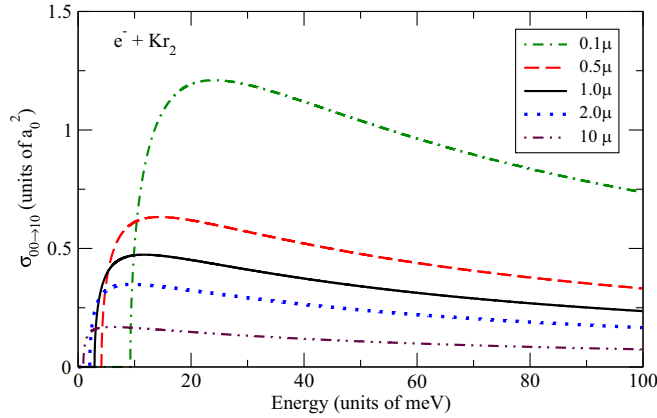

FIG. 9. Panel (a): Same as Fig. 7, but for $e^- + Xe_2$ considering the electron-atom scattering length $A = -5.13$. Panel (b): same as panel (a), but for electron-atom scattering length $A = -6.09$.

FIG. 10. Vibrational transition $00 \to 10$ cross sections considering different masses for the Kr_2 dimer calculated in the ZRP prescription. Dashed-dotted line: mass $0.1\mu \approx 7.64 \times 10^3$; dashed line: mass $0.5\mu \approx 3.82 \times 10^4$; solid line: results considering the original mass μ of the Kr_2 dimer; dotted line: mass $2.0\mu \approx 1.53 \times 10^5$; dashed-double-dotted line: mass $10\mu \approx 7.64 \times 10^5$.
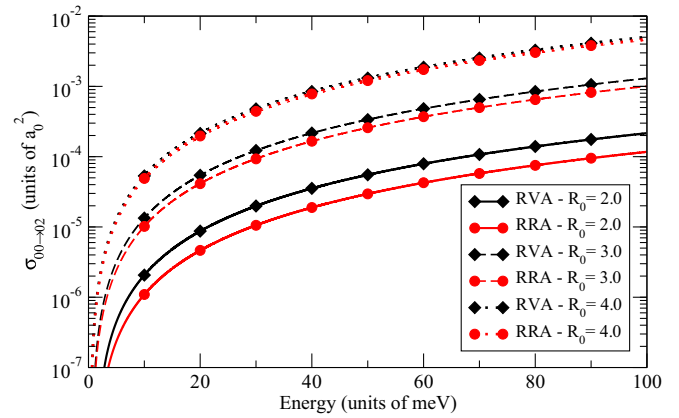

FIG. 11. Results for the $00 \to 02$ cross sections calculated in the RRA (lines with circles) and RVA (lines with diamonds) with different R_0 for a model dimer within the ZRP prescription. The parameters used are: mass $\mu = 1.0 \times 10^4$, vibrational constant $\omega_v = 1.0 \times 10^{-4}$, and electron-atom scattering length $A = 5.0$. Solid lines: results for $R_0 = 2.0$; dashed lines: results for $R_0 = 3.0$; dotted lines: results for $R_0 = 4.0$.

the mass, the larger the magnitude of the $00 \to 10$ cross section.

As we developed models considering different levels of sophistication, with special focus in the RRA and the RVA, we are able to study when such models give identical results for the rotational transition cross section. In other words, when should the vibrational couplings not be ignored in the calculation of the rotational cross sections? In fact, it is expected that the coupling between the rotational and vibrational states of the dimer affects the rotational transitions. For the dimers studied in this work, however, the difference between the results obtained within the RRA and RVA are smaller than $\sim 0.5\%$.

In order to visualize when the rovibrational coupling may considerably affect the results, we performed a calculation regarding a model molecular dimer for the pure rotational transition $00 \to 02$. The internuclear equilibrium distance R_0, and, therefore, the rotational constant B_r, has been varied. Meanwhile, the values considered are 1.0×10^4 for the dimer mass μ, 1.0×10^{-4} for the vibrational constant ω_v, and 5.0 for the electron-atom scattering length A. One can verify from Tables III and IV that these are typical values for the rare-gas dimers studied here.

The first value of internuclear distance considered was $R_0 = 4.0$, which gives $B_r = 3.31 \times 10^{-6}$, a value 2 orders of magnitude smaller than ω_v. From Fig. 11 it is seen that the results are practically indistinguishable. After, we performed calculations with lower values of R_0 in order to test what happens when values of B_r approach ω_v. We also show in Fig. 11 results for $R_0 = 2.0$, 3.0, corresponding to $B_r = 1.25 \times 10^{-5}$, 5.56×10^{-6}, respectively, calculated within the RRA and RVA. From this, one may notice that the difference between the outcomes produced by the RRA and RVA increases when the equilibrium distance decreases. This strongly suggests that the rovibrational coupling becomes more important as B_r approaches ω_v. In this case, the RVA shall provide results with greater accuracy.

V. SUMMARY AND CONCLUSIONS

The ZRP approximation has been used to investigate elastic and rovibrational excitation cross sections for electron scattering by van der Waals rare-gas dimers. The dimers are described as two rare-gas atoms under an internuclear constraint characterized by its molecular parameters. The electron-molecule interaction is described by a simple boundary condition, which, in its original prescription, depends on a parameter κ_0.

In order to go beyond the original ZRP prescription, the polarization effects have been included in the model inspired by the MERT. This new prescription has been called ZRPP, and it improves the results for electron-atom scattering when compared to those found in literature. This is an important improvement, once the quality of the electron-dimer results depends on the quality of the electron-atom results.

Considering the nuclear degrees of freedom of the target, three approximations have been considered. The simplest one is the fixed nuclei approximation. This enables us to calculate the elastic cross section for the electron dimer analytically. Interesting implications have been observed in this scenario, such as an equation for the molecular scattering length A_m, and also a linear dependence of the elastic cross section on the electron incident momentum in the ZRPP model, which is not registered in the pure ZRP.

The rigid rotor approximation was the second case considered. As in the fixed nuclei case, the cross section also can be calculated analytically. The direct comparison to the exact model of Ostrovsky and Ustimov [23] and with the adiabatic approximation led us to conclude that, in spite of using an approximated scattering wave function, the results provided by the ZRP give cross sections with lower magnitude but with similar energy dependence compared to the more sophisticated models. However, as we have shown, an analytical expression that accounts for the missing partial waves in the ZRP can be evaluated, generating a rescaled ZRP model. We

find that the scale factor, in the energy regime studied, does not depend on the energy of the incident electron.

Still working in the rigid rotor approximation, we have found that the ZRP and ZRPP models do not respect the principle of detailed balance (PDB) due to the approximated character of the scattering wave function. Nonetheless, the PDB is numerically respected once the adiabatic approximation is considered. Analyzing it, we have figured out it is interesting to chose the lower value between k_J and k_0 for the argument of the κ_0 parameter, since such a prescription enhances the agreement between the ZRP and ZRPP models for energies closer to the threshold.

The usual prescription to calculate electron-diatomic molecule rotational cross sections is the quadrupole Gerjuoy-Stein model (GS) [41]. Comparing the results obtained through ZRP to the GS results, we have observed that the rotational cross sections of the ZRP are larger in magnitude than the corresponding GS cross sections (except for the Xe_2 dimer). As the ZRP describes only short-range interactions, the results suggest that, different from the usual studied molecules such as H_2 and N_2, these are the preponderant ones in the rotational transitions for the electron-dimer collisions.

Following, we have developed calculations in the rovibrational approximation. Although we have not been able to present an analytical form for these, the matrix elements, in which the rovibrational coupling is present, are calculated analytically and the $0J_i \to nJ$ excitation cross section is computed numerically. The analytical nature of the ZRP method permitted us to investigate how the cross sections vary with the molecular parameters. We have found that the vibrational cross sections are affected by the dimer mass: the larger the mass, the lower the cross section. Nonetheless, the elastic and the rotational cross sections are insensitive to the oscillator mass.

Comparing the results calculated in the rigid rotor and rovibrational approximations for all dimers, we have found that the differences between the results for the rotational cross sections, evaluated in each approximation, are smaller than 0.5%. Using a model dimer with typical parameters, we have figured out that rovibrational couplings become important as long as the rotational constant B_r gets closer to the vibrational constant ω_v.

Finally, we have presented here an article addressing the electron scattering by van der Waals rare-gas dimers. Due to the improvement of the electron-single atom scattering description, we conclude that the ZRPP model shall provide more realistic elastic and inelastic cross sections.

ACKNOWLEDGMENTS

APPENDIX: MATRIX ELEMENTS

The matrix element present in Eq. (41) is

$$\langle n| \frac{e^{ik_{n'J}R}}{R}|n'\rangle = \int \Phi_n^*(R)\frac{e^{ik_{n'J}R}}{R}\Phi_{n'}(R)dR. \quad \text{(A1)}$$

In the harmonic approximation, the vibrational wave function $\Phi_n(R)$ is given by the eigenstates of the quantum harmonic oscillator

$$\Phi_n(R) = \frac{1}{\sqrt{2^n n!}}\left(\frac{\mu\omega_v}{\pi}\right)^{\frac{1}{4}}e^{-\mu\omega_v x^2/2}H_n(\sqrt{\mu\omega_v}x), \quad \text{(A2)}$$

where $x = R - R_0$, and the other variables are defined in the text. The matrix element of Eq. (A1) considering the eigenstates (A2) has been calculated by Gribakin up to leading order [24]:

$$\langle n|\frac{e^{ik_{n'J}R}}{R}|n'\rangle = \frac{e^{ik_{n'J}R_0}(-1)^{|n-n'|}}{R_0(R_0\sqrt{2\mu\omega_v})^{|n-n'|}}\sqrt{\frac{\max(n,n')!}{\min(n,n')!}}$$
$$\times \sum_{l=0}^{|n-n'|}\frac{(-ik_{n'J})^l}{l!}. \quad \text{(A3)}$$

The matrix element given by Eq. (13) with Eq. (41) as molecular wave functions becomes

$$\langle nJM|e^{i\vec{k}_{0J_i}\cdot\vec{R}/2}|0J_iM_i\rangle$$
$$= \int \Phi_n^*(R)Y_{JM}^*(\hat{R})e^{i\vec{k}_{0J_i}\cdot\vec{R}/2}\Phi_0(R)Y_{J_iM_i}(\hat{R})dRd\hat{R}. \quad \text{(A4)}$$

In order to uncouple the radial and angular part of the integral, we write $e^{i\vec{k}_{0J_i}\cdot\hat{R}R/2} = e^{i\vec{k}_{0J_i}\cdot\hat{R}R_0/2}e^{i\vec{k}_{0J_i}\cdot\hat{R}(R-R_0)/2}$. Both exponentials are, then, expanded using the well-known plane-wave expansion. In the spherical basis, this leads to

$$\langle nJM|e^{i\vec{k}_{0J_i}\cdot\vec{R}/2}|0J_iM_i\rangle$$
$$= (4\pi)^2 \sum_{c=0}^{\infty}\sum_{d=-c}^{c}\sum_{\gamma=0}^{\infty}\sum_{\nu=-\gamma}^{\gamma}i^{c+\gamma}j_\gamma\left(\frac{k_{0J_i}R_0}{2}\right)$$
$$\times Y_{cd}^*(\hat{k}_{0J_i})Y_{\gamma\nu}(\hat{k}_{0J_i})G_{JM\gamma\nu}^{J_iM_icd}I_n^{0c}, \quad \text{(A5)}$$

where the angular and radial integrals, respectively, are

$$G_{JM\gamma\nu}^{J_iM_icd} = \int Y_{JM}^*(\hat{R})Y_{\gamma\nu}^*(\hat{R})Y_{cd}(\hat{R})Y_{J_iM_i}(\hat{R})d\hat{R}, \quad \text{(A6)}$$

$$I_n^{0c} = \int_{-\infty}^{\infty}\Phi_n^*(x)j_c\left(\frac{k_{0J_i}x}{2}\right)\Phi_0(x)dx, \quad \text{(A7)}$$

where $x = R - R_0$, and $j_c(y)$ is the spherical Bessel function of order c. To calculate the angular integral (A6), we invoke the relation

$$Y_{ab}(\hat{R})Y_{\alpha\beta}(\hat{R}) = \sum_{A=|a-\alpha|}^{a+\alpha}\sum_{B=-A}^{A}\left[\frac{(2a+1)(2\alpha+1)}{4\pi(2A+1)}\right]^{\frac{1}{2}}$$
$$\times \langle a0\alpha0|A0\rangle\langle ab\alpha\beta|AB\rangle Y_{AB}(\hat{R}), \quad \text{(A8)}$$

and the solution of such an integral is

$$
G_{JM\gamma\nu}^{J_i M_i cd} = \sum_{A=\max(|J-\gamma|,|J_i-c|)}^{\min(J+\gamma,J_i+c)}
$$

$$
\times \sum_{B=-A}^{A} \left[\frac{(2J+1)(2\gamma+1)(2J_i+1)(2c+1)}{(4\pi)^2(2A+1)^2} \right]^{\frac{1}{2}}
$$

$$
\times \langle J0\gamma 0|A0 \rangle \langle JM\gamma\mu|AB \rangle
$$

$$
\times \langle J_i 0 c 0|A0 \rangle \langle J_i M_i cd|AB \rangle . \quad \text{(A9)}
$$

Using Eq. (A2) in (A7), the radial integral becomes

$$
I_n^{0c} = \left(\frac{\mu\omega_v}{2^n \pi n!} \right)^{\frac{1}{2}} \int_{-\infty}^{\infty} j_c \left(\frac{k_{0J_i} x}{2} \right) e^{-\mu\omega_v x^2} H_n(\sqrt{\mu\omega_v}x)dx. \quad \text{(A10)}
$$

In order to solve this integral, the first step is to write the Hermite polynomials as [50]

$$
H_n(\sqrt{\mu\omega_v}x) = n! \sum_{l=0}^{\frac{n-\xi_n}{2}} \frac{(-1)^{\frac{n-\xi_n}{2}-l}(2\sqrt{\mu\omega_v})^{2l+\xi_n}}{(2l+\xi_n)!\left(\frac{n-\xi_n}{2}-l\right)!} x^{2l+\xi_n}, \quad \text{(A11)}
$$

where

$$
\xi_n = \begin{cases} 0, & \text{for } n \text{ even;} \\ 1, & \text{for } n \text{ odd.} \end{cases} \quad \text{(A12)}
$$

The radial integral, using Eq. (A11) and writing the spherical Bessel function in terms of the Bessel function $J_a(y)$, becomes

$$
I_n^{0c} = \sum_{l=0}^{\frac{n+\xi_n}{2}} F_l^n \int_{-\infty}^{\infty} J_{c+\frac{1}{2}} \left(\frac{k_{0J_i} x}{2} \right) e^{-\mu\omega_v x^2} x^{2l-\frac{(-1)^n}{2}} dx, \quad \text{(A13)}
$$

with

$$
F_l^n = \left(\frac{\mu\omega_v n!}{2^n k_{0J_i}} \right)^{\frac{1}{2}} \frac{(-1)^{\frac{n-\xi_n}{2}-l}(2\sqrt{\mu\omega_v})^{2l+\xi_n}}{(2l+\xi_n)!\left(\frac{n-\xi_n}{2}-l\right)!}. \quad \text{(A14)}
$$

Following next, we use the identity $J_{a+1/2}(-x) = (-1)^a i J_{a+1/2}(x)$ in Eq. (A13) to get

$$
I_n^{0c} = \sum_{l=0}^{\frac{n+\xi_n}{2}} F_l^n [1+(-1)^{n+c}]
$$

$$
\times \int_0^{\infty} J_{c+\frac{1}{2}} \left(\frac{k_{0J_i} x}{2} \right) e^{-\mu\omega_v x^2} x^{2l-\frac{(-1)^n}{2}} dx. \quad \text{(A15)}
$$

The integral present in Eq. (A15) has an analytical solution [51]:

$$
\int_0^{\infty} J_{c+\frac{1}{2}} \left(\frac{k_{0J_i} x}{2} \right) e^{-\mu\omega_v x^2} x^{2l-\frac{(-1)^n}{2}} dx
$$

$$
= \frac{2\Gamma\left(\frac{1}{2}\left[c+\frac{1}{2}+2l-\frac{(-1)^n}{2}+1 \right] \right)}{k_{0J_i}(\sqrt{\mu\omega_v})^{(2l-\frac{(-1)^n}{2})}\Gamma(c+\frac{1}{2}+1)}
$$

$$
\times e^{-\frac{k_{0J_i}^2}{32\mu\omega_v}} M_{\frac{1}{2}(2l-\frac{(-1)^n}{2}),\frac{1}{2}(c+\frac{1}{2})}\left(\frac{k_{0J_i}^2}{16\mu\omega_v} \right), \quad \text{(A16)}
$$

where $M_{\mu,\nu}(y)$ is the Whittaker function of the first kind, and $\Gamma(y)$ is the Gamma function. This integral can be simplified using the asymptotic form of the spherical Bessel function for $k_{0J_i} \ll 1$ in Eq. (A7), once the problem is dealt with in the low-momentum regime. The expression obtained is

$$
I_n^{0c} = \left(\frac{k_{0J_i}}{2\sqrt{\mu\omega_v}} \right)^c \frac{\sqrt{k_{0J_i}/\pi}}{(2c+1)!!} \sum_{l=0}^{\frac{n-\xi_n}{2}} \frac{F_l^n}{\sqrt{\mu\omega_v}^{2l+\xi_n+1}} I_n^{lc}, \quad \text{(A17)}
$$

where

$$
I_n^{lc} = \int_{-\infty}^{+\infty} x^{2l+\xi_n+c} e^{-x^2} dx
$$

$$
= \frac{1}{2}[1+(-1)^{c+n}]\Gamma\left(\frac{2l+c+\xi_n+1}{2} \right). \quad \text{(A18)}
$$

[1] A. J. Marks, N. Murrell, and A. J. Stace, J. Chem. Soc. Faraday Trans. **87**, 831 (1991).

[2] R. Kalus, J. Chem. Phys. **109**, 8289 (1998).

[3] Y. Tanaka and K. Yoshino, J. Chem. Phys. **50**, 3087 (1969).

[4] Y. Tanaka and K. Yoshino, J. Chem. Phys. **57**, 2964 (1972).

[5] Y. Tanaka and K. Yoshino, J. Chem. Phys. **53**, 2012 (1970).

[6] Y. Tanaka, K. Yoshino, and D. E. Freeman, J. Chem. Phys. **59**, 5160 (1973).

[7] D. E. Freeman, K. Yoshino, and Y. Tanaka, J. Chem. Phys. **61**, 4880 (1974).

[8] P. Slavíček, R. Kalus, P. Paška, I. Odvárková, P. Hobza, and A. Malijevský, J. Chem. Phys. **119**, 2102 (2003).

[9] K. T. Tang and J. P. Toennies, J. Chem. Phys. **118**, 4976 (2003).

[10] M. S. Cybulski and R. R. Toczylowski, J. Chem. Phys. **111**, 10520 (1999).

[11] A. R. Janzen and R. A. Aziz, J. Chem. Phys. **107**, 914 (1997).

[12] M. Allan, J. Phys. B: At. Mol. Opt. Phys. **26**, L73 (1993).

[13] F. Blanco and G. García, J. Phys: Conf. Ser. **438**, 012012 (2013).

[14] J. Royal and A. E. Orel, Phys. Rev. A **72**, 022719 (2005).

[15] V. Ngassam and A. E. Orel, Phys. Rev. A **73**, 032720 (2006).

[16] J. Royal and A. E. Orel, Phys. Rev. A **73**, 042706 (2006).

[17] P. Lukáč, O. Mikuš, I. Morva, Z. Zábudlá, J. Trnovec, M. Morvová, and K. Hensel, Plasma Sources Sci. Technol. **21**, 065002 (2012).

[18] V. A. Ivanov and A. S. Prikhodjko, J. Phys. B: At. Mol. Opt. Phys. **24**, L459 (1991).

[19] J. Tennyson, Phys. Rep. **491**, 29 (2010).

[20] B. I. Schneider and T. N. Rescigno, Phys. Rev. A **37**, 3749 (1988).

[21] Y. N. Demkov and V. N. Ostrovskii, *Zero-Range Potentials and Their Applications in Atomic Physics* (Plenum Press, New York, 1988).

[22] G. F. Drukarev and I. Y. Yurova, J. Phys. B: At. Mol. Opt. Phys. **10**, 3551 (1977).

[23] V. N. Ostrovsky and V. I. Ustimov, J. Phys. B: At. Mol. Opt. Phys. **16**, 991 (1983).

[24] G. F. Gribakin, Nucl. Instrum. Methods Phys. Res., Sect. B **192**, 26 (2002).

[25] S. Leble and S. Yalunin, Phys. Lett. A **306**, 35 (2002).

[26] S. Leble and S. Yalunin, Rad. Phys. Chem. **68**, 181 (2003).

[27] T. F. O'Malley, L. Spruch, and L. Rosenberg, J. Math. Phys. **2**, 491 (1961).

[28] G. F. Gribakin and C. M. R. Lee, Nucl. Instrum. Methods Phys. Res., Sect. B **247**, 31 (2006).

[29] J. M. Blatt and J. D. Jackson, Phys. Rev. **76**, 18 (1949).

[30] H. A. Bethe, Phys. Rev. **76**, 38 (1949).

[31] B. Bransden and C. Joachain, *Physics of Atoms and Molecules* (Prentice Hall, Englewood Cliffs, NJ, 2003).

[32] T. F. O'Malley, L. Rosenberg, and L. Spruch, Phys. Rev. **125**, 1300 (1962).

[33] D. V. Fedorov and A. S. Jensen, J. Phys. A: Math. Gen. **34**, 6003 (2001).

[34] K. Shigemura, M. Kitajima, M. Kurokawa, K. Toyoshima, T. Odagiri, A. Suga, H. Kato, M. Hoshino, H. Tanaka, and K. Ito, Phys. Rev. A **89**, 022709 (2014).

[35] M. Kurokawa, M. Kitajima, K. Toyoshima, T. Kishino, T. Odagiri, H. Kato, M. Hoshino, H. Tanaka, and K. Ito, Phys. Rev. A **84**, 062717 (2011).

[36] T. F. O'Malley, Phys. Rev. **130**, 1020 (1963).

[37] J. Mitroy, Phys. Rev. A **66**, 022716 (2002).

[38] A. M. Arthurs and A. Dalgarno, Proc. Roy. Soc. A: Math. Phys. **256**, 540 (1960).

[39] W. Demtröder, *Atoms, Molecules and Photons: An Introduction to Atomic, Molecular and Quantum Physics* (Springer, New York, 2010).

[40] C. Joachain, *Quantum Collision Theory* (North-Holland, Amsterdam, 1975).

[41] E. Gerjuoy and S. Stein, Phys. Rev. **97**, 1671 (1955).

[42] A. G. Donchev, Phys. Rev. A **76**, 042713 (2007).

[43] M. W. Schmidt, K. K. Baldridge, J. A. Boatz, S. T. Elbert, M. S. Gordon, J. H. Jensen, S. Koseki, N. Matsunaga, K. A. Nguyen, S. Su, T. L. Windus, M. Dupuis, and J. A. Montgomery, J. Comput. Chem. **14**, 1347 (1993).

[44] K. A. Peterson, D. Figgen, E. Goll, H. Stoll, and M. Dolg, J. Chem. Phys. **119**, 11113 (2003).

[45] S. R. Hunter, J. G. Carter, and L. G. Christophorou, Phys. Rev. A **38**, 5539 (1988).

[46] T. M. Miller and B. Benderson, Adv. At. Mol. Phys. **13**, 1 (1978).

[47] T. P. Haley and S. M. Cybulski, J. Chem. Phys. **119**, 5487 (2003).

[48] P. Jerabek, O. Smits, E. Pahl, and P. Schwerdtfeger, Mol. Phys. **116**, 1 (2018).

[49] C. Focsa, P. F. Bernath, and R. Colin, J. Mol. Spectrosc. **191**, 209 (1998).

[50] R. Koekoek and R. F. Swarttouw, arXiv:math/9602214.

[51] I. S. Gradshteyn and I. M. Ryzhik, *Table of Integrals, Series, and Products* (Academic Press, London, 1980).